Journal of Materials Chemistry C

Accepted Manuscript

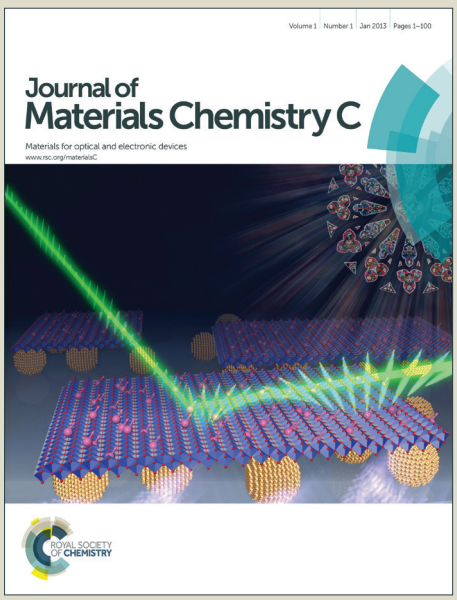

ROYAL SOCIETY OF CHEMISTRY

www.rsc.org/materialsC

Triple $Co^{II, III, IV}$ charge ordering and spin states in modular cobaltites: A systematization through experimental and virtual compounds

R. David[a], H. Kabbour[a*], P. Bordet[b,c], D. Pelloquin[d], O. Leynaud[b,c], M. Trentesaux[a] and O. Mentré[a]

[a] Unité de Catalyse et de Chimie du Solide, Université Lille Nord de France, Villeneuve d'Ascq, France

[b] Univ. Grenoble Alpes, Institut Néel, Grenoble, France

[c] CNRS, Institut Néel, Grenoble, France

[d] CRISMAT, Caen, France

Abstract

The series of modular compounds $[Ba_nCo_{2+n}O_{3n+2}][BaCo_6O_9]$ (n=1 to 3) including experimental and hypothetical terms, was investigated using DFT calculations and several experimental results. A systematic evolution of the electronic and magnetic states was evidenced along the series leading to ordered Co^{II}/Co^{III} versus mixed $Co^{III/IV}$ charge segregation in two distinct structural motifs. In essence, using different packing modes within the labile $[Ba_nCo_{2+n}O_{3n+2}]$ block, we have systematized the spin state dependence on the CoO_6 connectivity, i.e. corner-sharing (HS states) against face-sharing (LS states). We also show that the electronic and magnetic features of the $[BaCo_6O_9]$ blocks do not vary trough the series, (i.e. HS-Co^{II} and LS-Co^{III} charge ordering) whereas the $[Ba_nCo_{2+n}O_{3n+2}]$ blocks hold drastic changes from n=1 to 3. In particular, the later carries a mixed III/IV cobalt charge for $n \geq 2$. It leads to a triple valence cobalt state. For n=2, we experimentally observe at 4K a superstructure (2a, 2b, 2c) superstructure accompanied by a perfect $Co^{II}/Co^{III}/Co^{IV}$ charge ordering. The charge ordering occurs at Tt =160K and is accompanied by a transition in the electronic transport leading to a 2D-VRH behaviour below Tt.

Keywords: Cobaltites, magnetic properties, triple valence, charge ordering

Introduction

Cobalt oxides form an impressive field of investigation for new structures and fascinating properties like mixed ionic and electronic conductivity, superconductivity, thermoelectricity, magneto-resistivity and other features related to complex coupling between electrical and magnetic phenomena. It makes them increasingly interesting in the solid-state science community and their potential applications in various fields (fuel cells, data storage, gas sensors etc…) reinforce their attractiveness [1]. Such a variety of properties stems from the versatility of coordination, valence and spin states offered by cobalt ions. A representative example is given by the progressive incorporation of oxygen vacancies in the one-dimensional 2H-$BaCoO_3$ perovskite with columns of face-sharing low-spin $Co^{IV}O_6$ octahedra.[2] Upon reduction, anion-vacancies are segregated mainly in oxygen deficient [BaO_2] layers, so creating isolated blocks of face sharing low-spin CoO_6 octahedra (tetramers in 12H-$BaCoO_{\sim 2.83}$; trimers in 5H-$BaCoO_{\sim 2.8}$) with terminal high-spin CoO_4 tetrahedra. [3,4] In these compounds, the charge distribution was not clearly elucidated yet, but most probably mimics the specificities of related $Co^{III/IV}$ oxohalides with similar sub-units separated by [$BaOX_{1-\delta}$] (*X*= F, Cl) or [$Ba_2O_2Br_{1-\delta}$] layers instead of [BaO_2] in the oxides . The replacement of O^{2-} for X^- leads to a lower cobalt valence than in the parent oxides.[5–8] Trivalent high-spin ions (HS Co^{III}) occupy the terminal tetrahedral sites while the central octahedral columns adopt low spin mixed valent ions (LS-$Co^{III/IV}$) states. The segregation of the cobalt charges in these perovskite related compounds questions the possibility of trapping Co^{II}, Co^{III}, Co^{IV} triple valence states in particular modular structure combining perovskite blocks and distinct sub-units into more reduced systems. While total or partial charge ordering in distinct metal sites is not rare the disproportionation of mixed valent M^{n+} into three valence states is rather exceptional. In most oxides, transition metal *d* and O_{2P} states hybridize in the valence band leading to a mixed valence state between two bordering M^{n+} and M^{n+1} formal valences. To

the best of our knowledge, we can however cite a limited number of examples, , such as $Mn_{7.5}O_{10}Br_3$ which was demonstrated to display a triple valence $Mn^{2+/3+/4}$ through the study of different charge distribution scenarios and EELS experiments at the Mn $L_{2,3}$ edges. Different coordinations were assigned to the distinct valences, i.e. Mn^{II} (cubic sites), Mn^{III} (octahedral site) and Mn^{IV} (other octahedral site). [9,10] Similarly, the silicate $La_4Mn_5Si_4O_{22}$, related to the "Perrierite" mineral $La_4Mn_3Ge_{5.2}Si_{0.8}O_{22}$ [11], exhibits a triple valence of the manganese ($Mn^{II/III/IV}$) also confirmed by EELS experiments [12]. A triple valence scenario was also suggested in $Ba_8Mn_6Ca_2O_{23}$ and $Ba_7Mn_5Ca_2O_{20}$, however, in these particular compounds, with a charge ordering between tetrahedral Mn^{V} and octahedral $Mn^{IV}O_6$ in face sharing oligomers well separated by CaO_6 ions seems more plausible [13,14]. More recently, in $H_xLi_yCo_{3-\delta}$, electrode materials related to the Co_3O_4 spinel, the creation of Co vacancies in both tetrahedral and octahedral sites together with the incorporation of Li and H ions lead to a triple Co^{II}, Co^{III}, Co^{IV} valence. [15–17]

In this context, an opportunity for triple valence effect is given in the recent $[BaCoO_3]_n[BaCo_8O_{11}]$ series of compounds which were investigated for their structural, magnetic, transport properties [18–21] and also for their potentialities as SOFC's cathodes [22]. The above formula corresponds to a series of intergrowths between tuneable perovskite blocks (likely to stabilize $Co^{III/IV}$ valence) and $[BaCo_8O_{11}]$ motifs in which earlier works validated a perfect ordering between Co^{II} and Co^{III} crystallographic sites[18,19]. From n=1 to n=3, one can immediately observe that the main Co valence changes from $Co^{+2.66}$ to $Co^{>+3}$ which suggests possible [mixed $Co^{III/IV}$] and [ordered Co^{II}, Co^{III}] triple valence state in the two subunits, respectively. Here we show that this unique feature should be respected as soon as n≥2, and experimentally leads to triple valence full ordering for n=2 below 160 K. In this purpose, we used low-temperature XRD experiments and DFT calculations on different

experimental and hypothetical structures corresponding to n=1, 2 and 3. The handling of these series also enables to generalize magnetic configurations on each cobalt sites.

State of the art:

The known members of the series $[BaCoO_3]_n[BaCo_8O_{11}]$ are $Ba_2Co_9O_{14}$ (n=1) ($R\bar{3}m$), $Ba_3Co_{10}O_{17}$ (n=2) ($R\bar{3}m$) and $Ba_6(Ga,Co)_{13}O_{26}$ (n=5) ($P\bar{3}m1$) first reported from single crystal XRD analysis. The n=1 member can be prepared as a single-phase material and appears as an efficient materials for SOFC cathode.[22] The n=2 member is more problematic since, apart from single crystals, it could not be obtained exempt of a significant amount of $Ba_2Co_9O_{14}$. Electronic features of the n=5 compound are out of the scope of this paper since only single crystals have been obtained after incorporation of Ga^{III} ions, leading to charge redistribution. For n=1 and 2, the magnetic structures refined from powder neutron diffraction (PND) [18,19] show a repartition of HS Co^{II} and HS and LS $Co^{III/IV}$ in the two subunits. It is sketched in the figure 1a,b where the generic $[BaCoO_3]_n[BaCo_8O_{11}]$ formula is modified into $[Ba_nCo_{2+n}O_{3n+2}]$ $[BaCo_6O_9]$ by anticipation of future discussions. The former motifs are magnetically modified between n=1 and n=2 (shown in grey) while the $[BaCo_6O_9]$ units (shown in purple) are maintained unchanged. The refined local magnetic moments are reported on the figure 1.

- In the $[BaCo_6O_9]$ motifs, central $[CdI_2]$-like layers of edge-sharing octahedra contain LS Co^{III} surrounding HS Co^{II}. They are capped by HS Co^{II} tetrahedra.

- In the $[Ba_nCo_{2+n}O_{3n+2}]$ motifs, corner-sharing and/or face-sharing CoO_6 octahedra correspond to Co^{III} cations for n=1, (formal valence Co^{+3}) or mixed $Co^{III/IV}$ cations for n=2, (formal valence $Co^{+3.25}$) with evidence of LS and HS spin states depending on the connection type.

For those two so-called experimental compounds, these attributions [19] are supported by PND data, magnetic measurements and spin-polarized DFT calculations of the local Co moments.

Finally, we recall, that in our previous study of the *n*=2 compound, a transition appearing on both transport and magnetic properties was observed at ~160 K, while for *n*=1 no anomaly was detected.[18,19] A the origin of the transition, a possible Co^{III}/Co^{IV} charge ordering in the perovskite block was suggested for n=2.[19] At least the difficulty to synthesize members with n ≥2 play in favour of unstable valence states. It is relevant that no significant amount of oxygen vacancies was detected by PND for both *n*= 1 and *n*=2.

Experimental

Single crystal growth and X-rays diffraction at 4K

To obtain single crystals of n=2, the same procedure than the one described in [19] has been used. A large excess of K_2CO_3 was added to a mixture of $BaCO_3$ and Co_3O_4 and was heated to 850 °C for 72 h and cooled down to room temperature (5 °C/h down to 600 °C and then rapidly). The product was finally washed with boiling water to remove K_2CO_3. Black crystals with a hexagonal platelet shape (maximal size≈500x500x50 μm) have been selected for X-ray and XPS measurements.

The single crystal X-ray diffraction experiments were carried out using a Bruker-AXS Kappa ApexII diffractometer equipped with an Incoatec IμS microsource generator and AgKα radiation (λ= 0.56086 Å). This diffractometer is specially adapted to measurements down to about 3.5K[cryostat] [23]. More details are provided in the supplementary materials. Two data collections were carried out at 180K and 4.9K at a fixed χ=45° imposed by the two-axis mini goniometer geometry. Both consisted in two 180° φ-scans separated by a 60° ω-scan, using a 0.5° frame angle. Integrated intensities were extracted using the EvalCCD package [24]and corrected for anisotropic absorption effects using the SADABS program [25], including a θ-dependent spherical absorption correction.

Crystal chemistry Method and Calculation methods

We aim to perform a systematic analysis of the local geometry, local magnetic moments and most plausible charge ordering by extension of the experimental results (n=1 and 2) to hypothetical polytypes or original members related to n>2 plausible homologues. To build new polytypes, one should keep in mind the usual description of the hexagonal perovskite blocks based on (BaO_3) layers stacked in either a hexagonal (h) or cubic manner (c) with Co layers intercalated in the interstitial octahedral sites. We used the experimental structural models of H-$Ba_2Co_9O_{14}$ (n=1, R-3m), C-$Ba_3Co_{10}O_{17}$ (n=2, $R\bar{3}m$) and mixed C/H-$Ba_6(Ga,Co)_{13}O_{26}$ (n=5, P-3m1) where the H and C prefix pictures the hexagonal (h) or cubic (c) layer stacking in the central perovskite sub-unit (see supplementary S1). Basically, to model novel hypothetical terms, an artificial separation is introduced between the [$BaCo_6O_9$] entities for incorporation of additional cobalt and BaO_3 layers. The additional layers are disposed with various h or c stacking, leading to three hypothetical structures: (i) H-$Ba_3Co_{10}O_{17}$ (n=2) (ii) C-$Ba_4Co_{11}O_{20}$ (n=3) and (iii) H-$Ba_4Co_{11}O_{20}$ (n=3). The corresponding crystal structures are shown on the figure 2.

Density functional theory (DFT) calculations were performed using the Vienna *ab initio* simulation package (VASP) [26]. The calculations were carried out within the generalized gradient approximation (GGA) for the electron exchange and correlation corrections using the Perdew-Wang [27] functional and the projector augmented-wave method (PAW).[28] The full geometry optimizations were carried out using a plane wave energy cutoff of 550 eV. C-$Ba_3Co_{10}O_{17}$, H-$Ba_3Co_{10}O_{17}$, C-$Ba_4Co_{11}O_{20}$ and H-$Ba_4Co_{11}O_{20}$, we used 10, 12, 10 and 10 k points in the irreducible Brillouin zone, respectively. All structural optimizations converged with residual Hellman-Feynman forces on the atoms smaller than 0.03 eV/Å and led to meaningful structures regarding the distances and the local geometries. The relaxed structures were used for accurate total energies calculations and concomitantly access to the calculated magnetic moments. For the total energies calculations and Density of States (DOS), spin-

polarized (on a ferromagnetic configuration for simplicity purposes) were carried out using simple GGA approximation with no Hubbard term (U=0) added to avoid artificial stabilization of high spin states, starting with high moment values in all Co sites. The wigner-seitz radius used for cobalt ions is provided by the PAW potential files of VASP, *i.e.* 2.460 a.u. A plane wave energy cutoff of 400 eV and an energy convergence criterion of 10^{-6} eV were used in that case. For the hypothetical terms H-$Ba_3Co_{10}O_{17}$, C-$Ba_4Co_{11}O_{20}$ and H-$Ba_4Co_{11}O_{20}$, we used 28, 26 and 28 *k* points in the irreducible Brillouin zone, respectively. For validation purposes the experimental member C-$Ba_3Co_{10}O_{17}$ (n=2) was fully relaxed (atomic positions and cell parameters) using geometry optimizations (see supplementary S2). The experimental structure match well the optimized one, i. e. within a reasonable error expected for the GGA method. Besides the geometrical features, the validity of the deduced local magnetic moments on each Co ion was verified for H-$Ba_2Co_9O_{14}$ (n=1) and C-$Ba_3Co_{10}O_{17}$ (n=2) by comparison with the results of their refined magnetic structures as already reported in reference [19].

XPS

XPS experiments were carried out using a Kratos Analytical AXIS Ultra spectrometer. A monochromatized aluminum source (AlKα= 1486.6 eV) was used for excitation. The analyzer was operated in constant pass energy of 40 eV using an analysis area of approximately 700µm*300µm. Charge compensation was applied to compensate for the charging effect occurring during the analysis. The C1s hydrocarbon (285 eV) binding energy was used as internal reference. The spectrometer binding energy scale was initially calibrated against the Ag 3d (368.2 eV). Pressure was in the 10^{-9} Torr range during the experiments. Quantification and simulation of the experimental photo-peaks were carried out using CasaXPS software. Samples were analyzed both at low temperature and at room temperature. The low temperature analysis was carried out by cooling the sample with liquid nitrogen in the XPS

analyzing chamber. We probed the 3p levels of the Co since the habitual 2p levels interfere with the Ba 3d levels.

To perform an accurate study, in addition to single crystals of n=2, measurements have also been performed on reference compounds:

- Single crystals of $Ba_2Co_4ClO_7$ containing only $[Ba(Co^{II}/Co^{III})_6O_9]$ units separated by Cl based layers. The sample has been synthesized using the method described in [29].

- Single crystals of the 2H-$BaCoO_3$ compound which is formed of infinite chains of face sharing Co^{IV} octahedra. The sample has been synthesized using a stoechiometric ratio of $BaCo_3$ and Co_3O_4 in a KOH flux, heated at 400°C for 24 h in an alumina crucible.

TEM analyses

The experiments have been carried out with a JEOL 2010 FEG operating at 200kV (Cs=1nm) and equipped with a double tilt sample holder and an EDAX analyser. The simulated images have been calculated with the JEMS software.

Results and discussion

The DFT calculations converged with the magnetic repartition given in Table 1. All results regarding experimental and optimized lattice parameters, Co-O distances, magnetic moments and their attributions are gathered in the Table 1. From the two first columns, the reasonable matching between experimental and optimized structural and magnetic features can be verified, as discussed in the calculation methods section. The optimized structures (unit cell, atomic positions) of the hypothetical terms are given in S3. Concerning the calculated magnetic moments, discrepancies with the experimental ones (for n=1 and 2) are inherent to the calculation method and may also be due to our choice not to use the Hubbard (DFT+U) corrections for on-site electron repulsion, but could also stem from inaccuracy in PND refinement (especially for n=2 treated among a mixture). Especially, for octahedral positions

carrying a moment, greater discrepancies are observed while one would expect some scaling between experimental and theoretical values. Indeed, in absence of Hubbard terms specific for each geometry and/or accounting for possible spin-orbit coupling, one could expect different discrepancies. At least the distinction between HS and LS configurations further discussed is rather clear.

1) Systematic charge segregation into sub-units

In all compounds, **the $[BaCo_6O_9]$ blocks**, which combine the CdI_2-type triangular lattice of edge-sharing octahedra together with apical tetrahedra (in purple on the figure 1), can be considered as unchanged for all *n*-members independently of the *h/c* stacking in the next block : from the structural viewpoint, the Co-O bond distances remain nearly unchanged after structural relaxation for the concerned atoms, see Table 1, and fully compatible with the HS-Co^{II} (for Co1, and Co5) and LS-Co^{III} (for Co2) primary assignment for n=1 and 2 .[18, 19] This statement is further supported regarding the electronic features of this block. The calculated magnetic moments on octahedral Co1 (from 2.34 to 2.37μB), octahedral Co2 (0.06 to 0.14 μB) and tetrahedral Co5 (2.18 to 2.31 μB) suggest the preservation of this charge/spin distribution for all the series. In addition, the topology of the DOS is rather similar than previously reported results for $Ba_2Co_9O_{14}$ and $Ba_3Co_{10}O_{17}$ [18,19] (see supplementary S4).. It follows that a fixed mean charge per cobalt can be calculated as $Co^{+2.5}_{[BaCo6O9]}$ accordingly with the multiplicity of $Co1^{II}$, $Co2^{III}$, $Co5^{II}$ positions. Here, the $Co^{+2.5}$ conservation in the full series suggests electronic reorganization in the next $[Ba_nCo_{2+n}O_{3n+2}]$ subunit, to reach the mean cobalt valence for each individual compound.

The $[Ba_nCo_{2+n}O_{3n+2}]$ units include the central hexagonal perovskite block (Co3, Co6) and the terminal face-sharing octahedra (Co4) located between the tetrahedra. The unchanged charge ordering in $[BaCo_6O_9]$ blocks leads to the average oxidation state $Co^{+3}_{[BaCo3O5]}$, $Co^{+3.25}_{[Ba2Co4O8]}$ and $Co^{+3.4}_{[Ba3Co5O11]}$ for *n*=1, *n*=2 and *n*=3, respectively. The analysis of Co-O

bonds shows significant changes for all the concerned atoms between all members (*c*/*h* effect and *n* effect) which strongly suggest a variable mean oxidation state that may be favoured in perovskite related blocks. For instance for *h* stacking only (i.e. face sharing columns of octahedral), all mean Co3-O, Co6-O and Co4-O bond lengths decrease with *n* in good agreement with the cobalt valence in the $[Ba_nCo_{2+n}O_{3n+2}]$ sub-units.

Therefore a unified charge repartition occurs in the $[Ba_nCo_{2+n}O_{3n+2}]$ and $[BaCo_6O_9]$ sub-units. In $[BaCo_6O_9]$, Co^{II} and co^{III} cations coexist in a fully ordered manner. In the $[Ba_nCo_{2+n}O_{3n+2}]$ blocks, only Co^{III} exist at n=1 while a progressive oxidation into mixed $Co^{III/IV}$ appears for greater *n* members. It leads to an original triple valence state with segregation into distinct structural modules. The different charge segregation into $[Ba_nCo_{2+n}O_{3n+2}]$ and $[BaCo_6O_9]$ sub-units respectively may be related to specific ionic selectivity of each of them. Hence, the occupancy of the $[Ba_nCo_{2+n}O_{3n+2}]$ perovskite-related blocks by mixed Co^{III}/Co^{IV} states is typical of perovskite-related cobaltites including more "exotic" face-sharing oligomers in $BaCo^{IV}O_3$, $Ca_3Co^{III}{}_2O_6$, $BaCo^{III/IV}O_{3-x}$ and $BaCo^{III/IV}O_{3-x}X_y$ (X= F, Cl) oxo-halides.. On the opposite, it is questionable why the $[BaCo_6O_9]$ blocks retain a Co^{II}/Co^{III} ordering in the CdI_2-type layers on increasing the *n* order, since most of the related layered cobaltites display mixed Co^{III} or eventually $Co^{III/IV}$ lattices such as in the misfit $[Ca_2CoO_3][CoO_2]_{1.62}$ compound and layered A_xCoO_2 phases. Also in depleted triangular lattice such as the *Kagomé* lattice of spinel Co_3O_4, Co^{III} ions solely occupy the layers. However, in the full series of compounds investigated here, including the related $Ba_2Co_4XO_7$ which also contains isolated $[BaCo_6O_9]$ [29], one should recall that the voluminous $Co1^{II}O_6$ octahedra (Co-O~ 2.0 Å, see figure 1) is imposed by the face sharing with $Co4O_6$ of the next block. Therefore, similarly to $H_{1.34}Li_{0.14}Co^{II}{}_{0.61}[Co^{III}{}_{1.58}Co^{IV}{}_{0.14}]O_4$ nanospinel cobalt phases described in ref [15–17], the triple Co charge segregation occurs in well separated units and crystal sites.

An extra argument for the validity of our proposed charge distribution in the studied family of compounds is the increasing difficulty to synthesize the compounds on increasing *n*. This tendency can be summarized as follows: i) n=1: easy-solid state synthesis (powder and crystals[18,20] ii) n=2: preparation not yet achieved as a single phase material but possibility to grow single crystal [19,20] iii) $n > 2$ members have never been observed in absence of chemical doping [21]. In our study, we have been able to observe by high resolution electron microscopy (HREM) in a sample of formula $Ba_4Co_{11}O_{20}$, crystallites of the n=3 type. HREM images recorded for different samples prepared for increased *n* stoichiometries are given in the figure 3. The typical [100] oriented HREM images were obtained tuning the focus values. For a focus value close to 550nm, the [BaO_3] layers are emphasized and allow identification of the stacking mode in the perovskite block. As shown in figure 3a-b, for the two first members, $Ba_2Co_9O_{14}$ and $Ba_3Co_{10}O_{17}$ respectively, the [BaO_3] stacking sequences agree well with the experimental *hh* and *hch* configurations, respectively. It is noteworthy that stacking faults are regularly identified in the domains of the *n*= 2 sample (obtained systematically multiphased) [19]. In comparison with both previous members, in *n*= 3 the Ba positions respect the *hcch* configuration, as proven by the simulated images calculated from both relaxed models H or C (figure 3). Therefore, the experimental stabilization of $n>2$ domains seems therefore permitted but remain quite difficult to reproduce and observed scale up above crystallite sized areas.

Although this study mainly concerns a series of virtual compound, C-$Ba_3Co_{10}O_{17}$ is of strategical importance since it experimentally exist and validates an effective $Co^{II,\ III,\ IV}$ valence. Of course the synthesis difficulties most probably arise from triple valence equilibrium. We recall that the formula and discussion given above implies the absence of oxygen vacancies in the compounds. This was demonstrated in by PND refinement of the n=1 and 2 compounds [18, 19]..

2) *Triple $Co^{II/III/IV}$ charge Ordering in $Ba_3Co_{10}O_{17}$ (n=2).*

We have previously reported for n=2 single crystals, a strong anomaly observed on transport and magnetic properties at Tt ~160−170 K.[19] In this preliminary work, we have verified that below this temperature, the conductivity regime changes from an Arrhenius thermally activated to a 2D variable-range hopping (VRH) conduction type. A possible monoclinic distortion below Tt was investigated at 100 K from single crystal XRD, but remains highly hypothetical.

Using single crystal XRD data at T=4.9 K, a set of supercell spots has been observed. Their indexation involves a 8 fold cell trigonal cell with parameters 2a, 2c, referred to the room temperature trigonal unit cell. The extinction conditions for the R-bravais lattice (hk(i)l : -h+k+l =3n) are preserved though the superlattice. The supercell spots are emphasized on figure 4a. According to their weak intensities, it is not surprising that these spots have not been observed at 100K, while liquid helium temperature lowers scattering thermal effects.

The unit cell and orientation matrix obtained in the high temperature phase at 180K were applied to the 4.9K data and refined. Bragg reflection intensities were extracted after doubling the cell parameters within an 8 fold supercell. This procedure ensured a correct indexing of the reflections, despite the very large unit cell dimensions (a=11.367(3) Å, c=72.001(5) Å in SG $R\bar{3}m$).

Several models have been tested as given on the Table 2. In fact, for all "converging" models the final result is more or less similar, such that the R-3m model was preferred due to similar R-factor values while the number of refined parameters is clearly lowered. We paid a special attention to the agreement with the full data set (R_{all} =15.17%, wR_{all} =9.11%) since most of the satellites are below the observation threshold ($I<3\sigma(I)$). In this model, all Co atoms positions observed at room temperature are split into four different positions.

In the [$BaCo_6O_9$] block, the split of Co1 and Co2 leads to minor local distortion, while according to bond valence calculations, the oxidation states should remain unchanged, as expected from magnetic structure refined in the average cell at T=2K.[19] The Co5 tetrahedra show a more contrasted behaviour since half of them (Co5-2-1 and Co5-2-2) show contraction of the three axial bonds (1.9 $Å_{(RT)}$ → 1.8 $Å_{(4K)}$) while the other half (Co5-1-1 and Co5-1-2) are dilated (1.9 $Å_{(RT)}$ → 2.0 $Å_{(4K)}$) leading to BVS [30] close to +3 and +2 respectively. At least for all CoO_4 tetrahedra the apical Co-O remain nearly unchanged (1.9Å) which suggest that the tetrahedral distortion below Tt mimics those of the neighbour corner-sharing $Co4O_6$ octahedra, discussed below. Indeed, in agreement with the calculated/experimental values of the tetrahedral moments, the most probable scenario preserves the HS-Co^{II} state of the Co5 tetrahedra.

In the [$Ba_nCo_{2+n}O_{3n+2}$] units, the atomic rearrangement is drastic as depicted by arrows showing the shifts and labels of the typical distances in the figure 4b. The Co-Co distances inside the face-sharing dimers remain roughly similar than at room temperature, so that the reorganization is mediated by oxygen shifts.. In fact, for 75% of the concerned CoO_6 octahedra the off-centering present at room temperature is preserved and even slightly increased. Strikingly, for the last 25% (Co4-1-1 and Co4-1-2), the low temperature configuration involves strikingly short Co-O bonds (3x ~1.8 Å and 3x~1.9 Å). The BVS shows a Co^{III}/Co^{IV} charge ordering. In details, the segregation into three Co^{III} for one Co^{IV} agrees perfectly with the $Co^{+3.25}$ valence calculated within these sub-units and suggested above. It leads to a perfect ordering of $Co^{II}/Co^{III}/Co^{IV}$ charges in a complex manner as depicted in the figure 4. It is also in excellent correlation with the abrupt increase of the resistivity and of the transport anisotropy estimated by $\rho_c/\rho_{(a,b)}$ [19] below Tt, see figure 5. In essence, the Co^{III}/Co^{IV} charge disproportionation is mainly expected to block the electron hopping along the c axis, while the transport in the unchanged Co^{II}/Co^{III} layers should be only

weakly affected. We recall that the conductivity change into a 2D-VRH regime below Tt was experimentally fitted, but remained unexplained in absence of an accurate low temperature structural model.[19]

For further experimental evidence of the triple valence state, we carried out XPS measurements on $Ba_3Co_{10}O_{17}$ by comparison with pertinent cobalt compounds. Unfortunately, due to overlapping of the informative Co 2p and Ba 3d spectra, we were limited to the study of the weaker poorly resolved Co 3p peaks. The $Ba_3Co_{10}O_{17}$ spectra decomposition could be done using the references $Ba_2Co_4ClO_7$ (containing only $[Ba(Co^{II}/Co^{III})_6O_9]$ units) and $BaCo^{IV}O_3$ (supplementary fig. S5). $BaCoO_3$ proportion can be evaluated to 20% maximum. It suggests the presence of Co^{IV}, however, a spectral decomposition using only $Ba_2Co_4ClO_7$ (ordered Co^{II}/Co^{III} states) also describes rather well the $Ba_3Co_{10}O_{17}$ spectra, even though a slightly lower agreement. It means that these results should be taken with caution and we cannot definitely state from XPS analysis about the charge distribution in $Ba_3Co_{10}O_{17}$. Finally, significant modification of XPS spectra have been observed between 77 K (below Tt, mixed $Co^{III/IV}$ state in the perovkite sub-units) and room temperature (above Tt, charge ordered Co^{III}/ Co^{IV} states in the perovskite sub-units) (fig. S5).

3) Generalized cobalt Spin states In the $[Ba_nCo_{2+n}O_{3n+2}]$ units.

The most important changes concern the systematic null or very weak values of moments found for all face-sharing octahedra (hexagonal layers, LS-$Co^{III/IV}$) against sizeable moments (cubic layers, HS-$Co^{III/IV}$, M=1.5-2.9 μ_B/Co) when corner-sharing is involved. Spin states can be deduced from the DOS topologies projected on the *d*-states of the Co atoms and are associated to the calculated values of magnetic moments (figure in S4 and table 1). Our calculations reproduce well the moments experimentally observed in *n*=1 and *n*=2. In our previous report [19], we argued that the introduction of cubic layers in *n*=2 induces a release of

the internal pressure leading to the low spin → high spin crossover. The hypothetical phases follow the same trends and confirm the systematization of LS for *h* stacking versus HS for *c* stacking in $[Ba_nCo_{2+n}O_{3n+2}]$ Also for *h*-stacking, we note that, though weak, the mean magnetic moment hold by the linear columns (trimers for n=1, tetramers for n=2 and pentamers for n=3) increases with *n* as expected from a progressive replacement of LS-Co^{III} (S=0) for LS-Co^{IV} (S=1/2). After averaging of the cobalt moment in these blocks, taking into account the relative multiplicity of Co3, 4, 6 sites we find ~$0.2_{\mu B}$ $(n=1)_{hh}$→~$0.3_{\mu B}$ $(n=2)_{hhh}$→~$0.4_{\mu B}$ $(n=3)_{hhhh}$ .. A similar evolution is calculated for compounds built on cubic layers, but in such cases HS CoO_6 contributions are involved. Concerning the systematization of LS(h) versus HS(c) cobalt spins, it is in perfect agreement with LS cations reported for cobaltites of the literature that contain linear chains of face-sharing octahedra ($BaCoO_3$ [31,32], $BaCoO_{3-\delta}$ [3,4,33], $Ca_3Co_2O_6$ [34], $Ba_6Co_6F_{0.93}O_{16}$ and $Ba_5Co_5F_{0.77}O_{12.88}$ oxy-chlorides. [35] It most probably involves crystal field splitting due to trigonal distortion. For instance in $BaCoO_3$, it was stated that the Co^{IV} d^5 ions are embedded in a trigonally distorted CoO_6 leading to a LS-Co^{IV} ($t_{2g}^5e_g^0$, *S*=1/2) situation. However, the local electronic structure depends on a multitude of parameters, namely, the relative strength and the interplay of the oxygen crystal field, the direct Co-Co bonding, the spin-orbit coupling, and the trigonal distortion. Our calculations allow to systematize this versatile magnetic configuration inside CoO_6 as a function of the connectivity type for the full $[Ba_nCo_{2+n}O_{3n+2}][BaCo_6O_9]$ series with related crystal structures and could be considered as a postulat.

Conclusion

In this paper, we have investigated the crystalline structures and associated electronic features within the homologous series $[Ba_nCo_{2+n}O_{3n+2}][BaCo_6O_9]$. In absence of a sufficient number of experimental compounds, our strategy consists of the virtual building and

calculations on new members for systematization. From member *n*=1 to 3, the labile perovskite block holds the electronic adjustment. We have shown that the stacking sequence (either hexagonal or cubic) is responsible for the magnetism in the later block, which was confirmed for all terms. Basically, the hexagonal packing leads to face sharing octahedra with shorter distances than the cubic one; this internal pressure associated with the local trigonal distortion favors a low spin configuration of the cobalt ions. On the contrary, the cubic packing allows high spin configuration of the Co ions in the perovskite block leading to 3D magnetism. The electronic adjustment from *n*=1 to 3 gives rise to a triple valence II/III/IV, which is a rare phenomenon. As the [$BaCo_6O_9$] block is not altered in the whole series (average charge…), Co^{IV} appear in the complementary block to fulfill the charge equilibrium. The experimental study of the *n*=2 compound $Ba_3Co_{10}O_{17}$ (cubic stacking) highlights a low temperature distortion giving rise to further charge ordering within a triple valence state as deduced from our predictions.

Acknowledgments: S. Curelea is thanked for providing sample for TEM. R. David thanks ENS Lyon for financial support. The CRI of the University Lille 1 is thanked for providing computation resources. This work was carried out under the framework of the MAD-BLAST project supported by the ANR (Grant ANR-09-BLAN-0187-01).

Supporting Information: S1 (Model structures), S2 (Optimization of the experimental n= 2 member), S3 (Hypothetical structures crystallographic data), S4 (Density of states), S5 (XPS measurements) and S6 (Low temperature single crystal XRD). This material is available free of charge via the Internet at http://pubs.acs.org

References

(1) Raveau, B.; Seikh, M. *Cobalt oxides: from crystal chemistry to physics*; Wiley-VCH: Weinheim, 2012.
(2) Taguchi, H.; Takeda, Y.; Kanamaru, F.; Shimada, M.; Koizumi, M. *Acta Crystallogr. B* **1977**, *33*, 1298.
(3) Jacobson, A. J.; Hutchison, J. L. *J. Solid State Chem.* **1980**, *35*, 334.
(4) Parras, M.; Varela, A.; Seehofer, H.; González-Calbet, J. M. *J. Solid State Chem.* **1995**, *120*, 327.
(5) Yamaura, K.; Young, D. P.; Siegrist, T.; Besnard, C.; Svensson, C.; Liu, Y.; Cava, R. J. *J. Solid State Chem.* **2001**, *158*, 175.
(6) Tancret, N.; Roussel, P.; Abraham, F. *J. Solid State Chem.* **2005**, *178*, 3066.
(7) Ehora, G.; Renard, C.; Daviero-Minaud, S.; Mentré, O. *Chem. Mater.* **2007**, *19*, 2924.
(8) Kauffmann, M.; Roussel, P. *Acta Crystallogr. B* **2007**, *63*, 589.
(9) Euzen, P.; Leone, P.; Mansot, J. L.; Bonneau, P.; Palvadeau, P.; Queignec, M. *Mater. Res. Bull.* **1992**, *27*, 1423.
(10) Mansot, J. L.; Leone, P.; Euzen, P.; Palvadeau, P. *Microsc. Microanal. Microstruct.* **1994**, *5*, 79.
(11) Taviot-Guého, C.; Chopinet, C.; Palvadeau, P.; Léone, P.; Mozdzierz, N.; Rouxel, J. *J. Solid State Chem.* **1999**, *147*, 247.
(12) Guého, C.; Mansot, J. L.; Léone, P.; Giaquinta, D.; Palvadeau, P. *ICEM 13-Paris* **1994**.
(13) Floros, N.; Michel, C.; Hervieu, M.; Raveau, B. *J. Solid State Chem.* **2002**, *168*, 11.
(14) Floros, N.; Michel, C.; Hervieu, M.; Raveau, B. *Chem. Mater.* **2000**, *12*, 3197.
(15) Godillot, G.; Guerlou-Demourgues, L.; Croguennec, L.; Shaju, K. M.; Delmas, C. *J. Phys. Chem. C* **2013**, *117*, 9065.
(16) Godillot, G.; Huo, H.; Ménétrier, M.; Bourgeois, L.; Guerlou-Demourgues, L.; Delmas, C. *J. Phys. Chem. C* **2012**, *116*, 26598.
(17) Godillot, G.; Guerlou-Demourgues, L.; Taberna, P.-L.; Simon, P.; Delmas, C. *Electrochem. Solid-State Lett.* **2011**, *14*, A139.
(18) Ehora, G.; Daviero-Minaud, S.; Colmont, M.; André, G.; Mentré, O. *Chem. Mater.* **2007**, *19*, 2180.
(19) David, R.; Pautrat, A.; Kabbour, H.; Sturza, M.; Curelea, S.; André, G.; Pelloquin, D.; Mentré, O. *Chem. Mater.* **2011**, *23*, 5191.
(20) Sun, J.; Yang, M.; Li, G.; Yang, T.; Liao, F.; Wang, Y.; Xiong, M.; Lin, J. *Inorg. Chem.* **2006**, *45*, 9151.
(21) Pelloquin, D.; Pérez, O.; Martinet, G.; Hébert, S.; Maignan, A. *Chem. Mater.* **2007**, *19*, 2658.
(22) Rolle, A.; Preux, N.; Ehora, G.; Mentré, O.; Daviero-Minaud, S. *Solid State Ion.* **2011**, *184*, 31.
(23) Fertey, P.; Argoud, R.; Bordet, P.; Reymann, J.; Palin, C.; Bouchard, C.; Bruyère, R.; Wenger, E.; Lecomte, C. *J. Appl. Crystallogr.* **2007**, *40*, 526.
(24) Duisenberg, A. J. M.; Kroon-Batenburg, L. M. J.; Schreurs, A. M. M. *J. Appl. Crystallogr.* **2003**, *36*, 220.
(25) *SADABS: Area-Detector Absorption Correction*; Siemens Industrial Automation, Inc.: Madison, WI, 1996.
(26) Kresse, G.; Furthmüller, J. *Vienna Ab-initio Simulation Package (VASP)*; Institut für Materialphysik: Vienna (http://cms.mpi.univie.ac.at/vasp), 2004.
(27) Perdew, J. P.; Wang, Y. *Phys. Rev. B* **1992**, *45*, 13244.
(28) Kresse, G.; Joubert, D. *Phys. Rev. B* **1999**, *59*, 1758.
(29) Kauffmann, M.; Tancret, N.; Abraham, F.; Roussel, P. *Solid State Sci.* **2007**, *9*, 885.
(30) Brese, N. E.; O'Keeffe, M. *Acta Crystallogr. B* **1991**, *47*, 192.
(31) Pardo, V.; Blaha, P.; Iglesias, M.; Schwarz, K.; Baldomir, D.; Arias, J. E. *Phys. Rev. B* **2004**, *70*, 144422.
(32) Yamaura, K.; Cava, R. J. *Solid State Commun.* **2000**, *115*, 301.
(33) Boulahya, K.; Parras, M.; González-Calbet, J. M.; Amador, U.; Martínez, J. L.; Tissen, V.; Fernández-Díaz, M. T. *Phys. Rev. B* **2005**, *71*, 144402.

(34) Fjellvåg, H.; Gulbrandsen, E.; Aasland, S.; Olsen, A.; Hauback, B. C. *J. Solid State Chem.* **1996**, *124*, 190.
(35) Mentré, O.; Kabbour, H.; Ehora, G.; Tricot, G.; Daviero-Minaud, S.; Whangbo, M.-H. *J. Am. Chem. Soc.* **2010**, *132*, 4865.

TABLES AND FIGURES

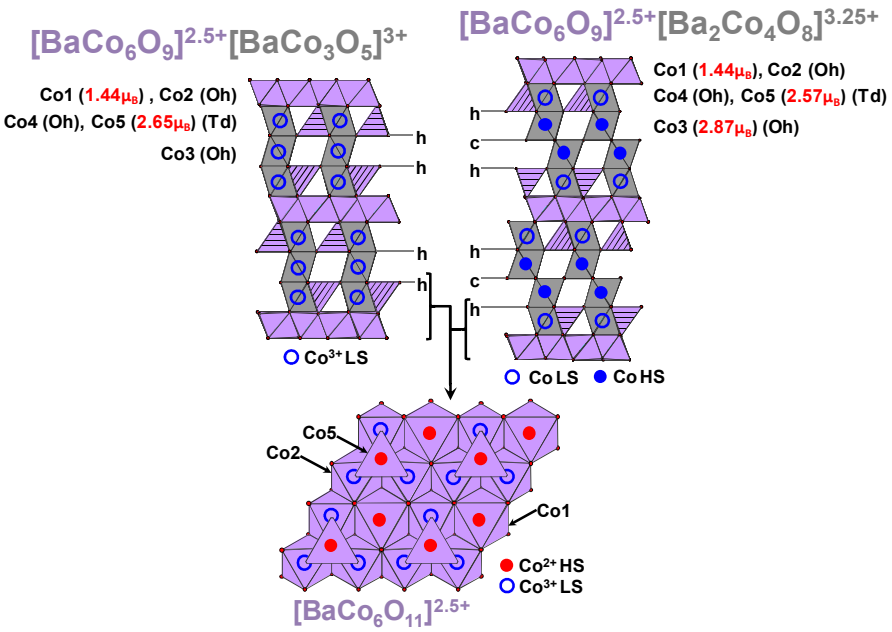

Figure 1. Comparison of $Ba_2Co_9O_{14}$ and $Ba_3Co_{10}O_{17}$ experimental structures and projection of the CoO_2 layer of the CdI_2 structural type. The magnetic moments obtained from neutron diffraction experiments are given for the cubic n=1 ($Ba_2Co_9O_{14}$) and n=2 ($Ba_3Co_{10}O_{17}$) polytypes.

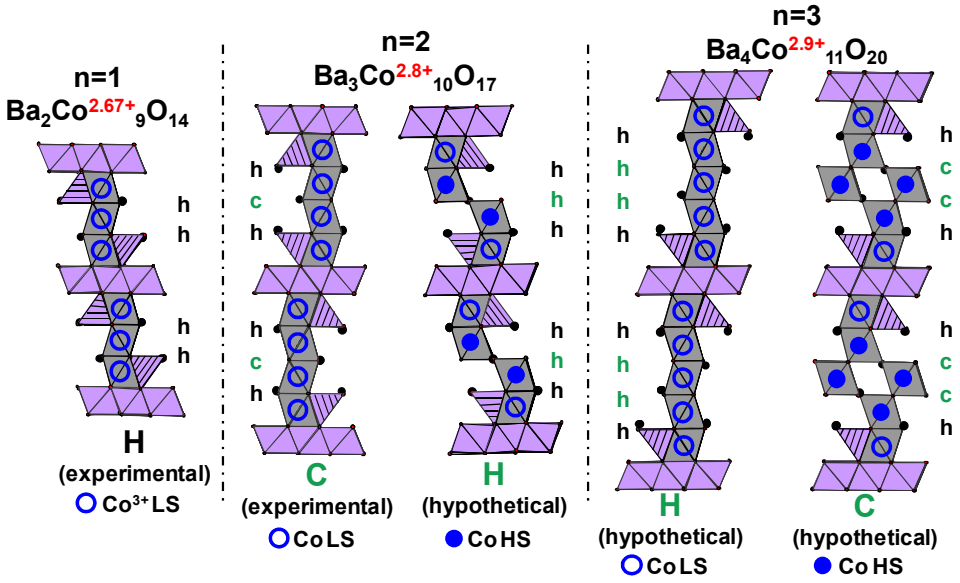

Figure 2. Structure of the experimental and hypothetical terms (n=1 to 3) with either hexagonal (H) or cubic (C) packing of the perovskite block. The stacking sequence for the

later is indicated in each case as well as magnetic cobalt atoms states (empty blue circles for low-spin state and filled blue circles for high-spin state) and the average oxidation state.

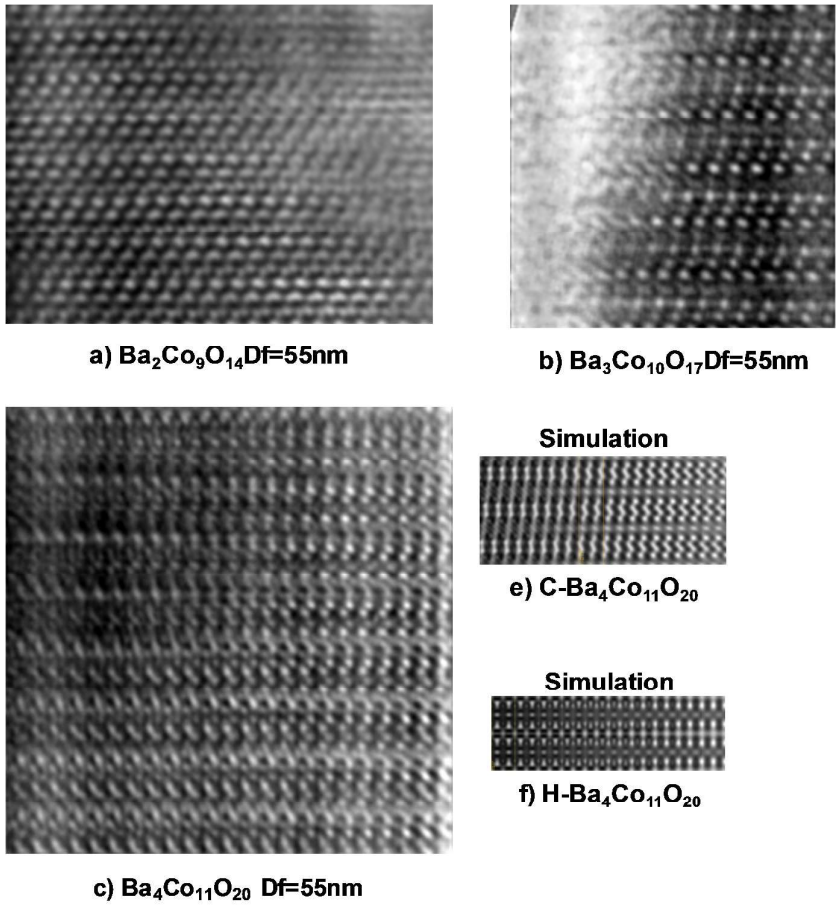

Figure 3. Experimental HREM images of (a) $Ba_2Co_9O_{14}$, (b) $Ba_3Co_{10}O_{17}$ and (c) $Ba_4Co_{11}O_{20}$ compared to simulated images in e) $P\bar{3}m1$ and f) $P\bar{3}$ space groups.

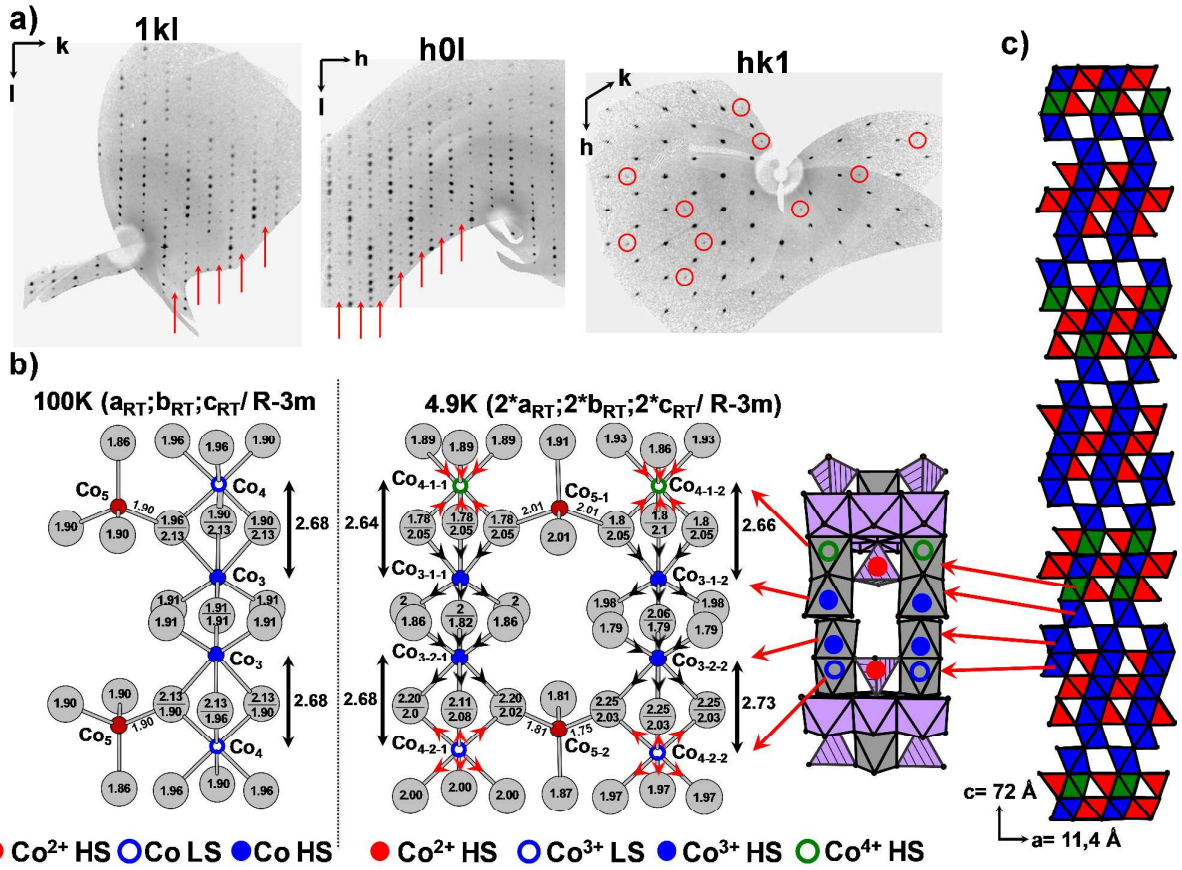

Figure 4. a) Diffraction patterns obtained on a single crystal of $Ba_3Co_{10}O_{17}$ at 4.9 K showing the appearance of superstructure spots in the (1kl) plane, (h0l) plane and (hk1) plane. The red arrows and circles highlight the superstructure spots. b) Structure of the low temperature (4.9K) form of $Ba_3Co_{10}O_{17}$, details of Co3, Co4 and Co5 evolution from 100 K to 4.9 K (distances are given in Å). c) Description of the charge order in the whole cell at 4.9 K.

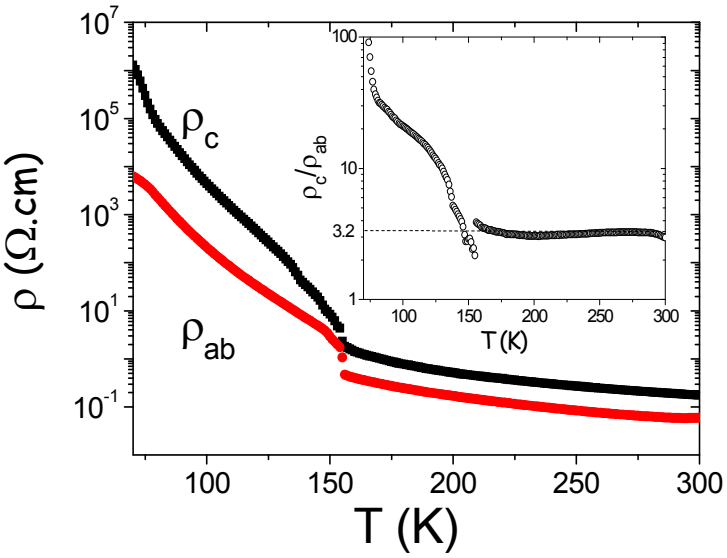

Figure 5. Single-crystal perpendicular (black) and in-plane (red) resistivity as a function of the temperature T (K). The inset shows the $\rho_c/_{ab}$ ratio as a function of the temperature T

Table 1. Comparison of the Co-O distances and magnetic moments in the *n*= 1 to 3 members.

		n=1*	n=2 cubic*	n=2 hexa	n=3 cubic	n=3 hexa
Standing block $[BaCo_6O_9]$ (experimental in red)	Co1 Octa.	6x2.075(2) 1.44/2.34 μB $Co^{II}_{(HS)}$	6x2.077(4) 6x1.9943 1.44/2.37 μB $Co^{II}_{(HS)}$	6x(1.9882/1.9879) 2.34 μB $Co^{II}_{(HS)}$	6x1.9884 2.36 μB $Co^{II}_{(HS)}$	6x1.9856 2.34 μB $Co^{II}_{(HS)}$
	Co2 Octa.	2x1.911(3) 4x1.923(3) 0/0.06 μB $Co^{III}_{(BS)}$	2x1.902(4) 2x1.9258 4x1.924(5) 4x1.9016 0/0.1 μB $Co^{III}_{(BS)}$	2x(1.9284/1.9275) 4x(1.9000/1.9023) 0.1 μB $Co^{III}_{(BS)}$	2x1.9274 4x1.8969 0.14 μB $Co^{III}_{(BS)}$	2x1.9370 4x1.8971 0.13 μB $Co^{III}_{(BS)}$
	Co5 Tetra	1x1.913(5) 3x1.924(4) 2.65/2.24 μB $Co^{II}_{(HS)}$	1x1.864(7) 1x1.8854 3x1.894(4) 3x1.8473 2.57/2.31 μB $Co^{II}_{(HS)}$	1x(1.9087/1.9041) 3x(1.8550/1.8551) 2.25 μB $Co^{II}_{(HS)}$	1x1.8900 3x1.8322 2.18 μB $Co^{II}_{(HS)}$	1x1.9263 3x1.8446 2.25 μB $Co^{II}_{(HS)}$
Changing block $[Ba_nCo_{2+n}O_{2+3n}]$ (experimental in red)		$[BaCo_3O_5]^{+3}$	$[Ba_2Co_3O_8]^{+3.25}$	$[Ba_2Co_3O_8]^{+3.25}$	$[Ba_3Co_4O_{11}]^{+3.4}$	$[Ba_3Co_4O_{11}]^{+3.4}$
	Co3 central	6x1.954(3) 0/0.3 μB $Co^{III}_{(BS)}$	3x1.913(1) 3x1.9006 3x2.135(4) 3x2.1619 2.87/1.93 μB $Co^{III/IV}_{(HS)}$	3x(1.9159/1.9158) 3x(2.0271/2.0229) 0.45 μB $Co^{III/IV}_{(BS)}$	3x1.8706 3x2.2055 1.43 μB $Co^{III/IV}_{(HS)}$	3x1.8985 3x2.0098 0.56 μB $Co^{III/IV}_{(BS)}$
	Co4 edge	3x1.926(2) 3x1.949(2) 0/0.14 μB $Co^{III}_{(BS)}$	3x1.927(4) 3x1.9047 3x1.958(5) 3x2.0552	3x(1.9142/1.9150) 3x(2.0400/2.0430) 0.19 μB $Co^{III/IV}_{(BS)}$	3x1.8898 3x2.0512 0.02 μB $Co^{III/IV}_{(BS)}$	3x1.9068 3x2.0327 0.26 μB $Co^{III/IV}_{(BS)}$

			0/0.18 µB $Co^{III/IV}_{(BS)}$			
	Co6 intermed				**6x2.0204 1.98 µB** $Co^{III/IV}_{(HS)}$	**6x1.9295 0.31 µB** $Co^{III/IV}_{(BS)}$

(*) The DFT calculated magnetic moments for the experimental n=1 $Ba_2Co_9O_{14}$ and n=2 cubic $Ba_3Co_{10}O_{17}$ are taken from reference 19.

Table 2. Refinements results in different space groups for the low temperature structure of $Ba_3Co_{10}O_{17}$

Space groupe	**R$\bar{3}$m**	**R32**	**R3m**	**R$\bar{3}$**	**R3**	**C2/m**
a (Å)	**11.367**	11.367	11.367	11.367	11.367	19.688
b (Å)/□(°)	**11.367**	11.367	11.367	11.367	11.367	11.367/105.29
c (Å)	**72.001**	72.001	72.001	72.001	72.001	24.881
sin(θ)/λ limit	**0.7**	0.7	0.7	0.7	0.7	0.7
Indpdt Reflections [I>3σ(I)]/tot	**813/2907**	1409/5121	1193/4459	1254/5116	1767/7658	3663/11272
R_{obs}/R_{all}	**4.52/15.17**	5.99/17.07	4.91/15.39	4.68/17.31	4.93/17.43	7.76/18.11
wR_{obs}/wR_{all}	**4.12/9.11**	4.56/10.22	4.36/9.05	4.17/10.13	4.48/17.43	7.06/10.39
GOF_{obs}/GOF_{all}	**1.44/1.64**	0.89/1.02	1.55/1.60	1.40/1.64	1.57/1.63	1.23/1.02
Parameters	**76**	118	157	118	241	194
Weighting scheme	**Unit**	Unit	Unit	Unit	Unit	Unit
max/min Δρ (e/Å^3)	**7.09 /-6.23**	5.53/-7.24	7.09/-7.02	6.7/-6.95	5.83/-7.6	5.48/-7.02
Ba Indep	**6**	6	12	6	12	9
U_{iso}	**fixed**	fixed	fixed	fixed	fixed	fixed
Co Indep	**20**	22	34	20	36	32
U_{iso}	**fixed**	fixed	fixed	fixed	fixed	fixed
O Indep	**19**	24	38	24	44	41
U_{iso}	**fixed**	fixed	fixed	fixed	fixed	fixed
Converged	**yes**	no	yes	Yes	No	yes

Table 3. Structure and refinement parameters of the low temperature distortion of $Ba_3Co_{10}O_{17}$

Crystal (T= 4.9 K)	
Formula	$Ba_3Co_{10}O_{17}$
Molar weight (g/mol)	848.9
Symmetry	Rhombohedric
Space group	$R\bar{3}m$
Unit cell (Å)	a = 11.367(3)
	c= 72.001(5)
Volume	8056.768(5) $Å^3$
Z	24
Data Collection	
Equipment	Bruker-AXS Kappa ApexII
Λ (Mo Kα (graphite mono-chromator); Å)	0.56087
Density calc. (g/cm^3)	6.296
Crystal dimensions (μm)	120x95x145
Color	black
Scan mode	ω, φ
θ (min-max) (°)	4.41-33
μ (mm^{-1}; for λ Kα = 0.7107 Å)	20.732
T_{min}/T_{max}	0.5118/0.7460
R(int) (%)	9.86
Recording reciprocal space	-22≤h≤21, -21≤k≤21,-98 ≤l≤139
Number of measured reflections	49949
Nbr of independent reflections ($I > 3\sigma(I)$), total)	2907/813
Refinement	
Number of refined parameters	76
Refinement method, program	Least squares on F
Weighting sheme	Unit
R1(F)[$I > 3\sigma(I)$]/R1(F^2) [all data, %]	4.52 /15.17
$wR^2(F^2)$ [$I > 3\sigma(I)$]/wR2(F^2) [all data, %]	4.12/9.11
GOF	1.64
Max/Min residual electronic density (e^-/ $Å^3$)	6.99/-7.12

Table 4. Atomic positions for the low temperature structure of $Ba_3Co_{10}O_{17}$. The thermal displacement parameters were fixed to 0.01 Å².

Atom	Wyck.	x	y	z
Ba1	6c	0.6667	0.3333	0.08324(3)
Ba2	18h	0.16957(7)	0.33914(13)	0.083705(17)
Ba3	18h	0.33163(13)	0.16582(7)	0.117618(17)
Ba4	6c	0	0	0.04922(3)
Ba5	18h	0.50110(7)	0.49890(7)	0.049913(17)
Ba6	6c	0.3333	0.6667	0.11701(3)
Co1-1-1	9d	-0.1667	0.1667	0.1667
Co1-1-2	3b	0	0	0
Co1-2-1	3a	0.0847(3)	0.4181(3)	0.1667
Co1-2-2	9e	-0.1655(3)	0.41724(16)	0.16690(4)
Co2-1-1	18g	0	0	0.09756(7)
Co2-1-2	18h	-0.16571(16)	0.16571(16)	0.03281(4)
Co2-2-1	18f	0	0	0.13425(7)
Co2-2-2	18h	0.16740(16)	0.3348(3)	0.03943(4)
Co3-1-1	6c	0.16714(16)	0.3343(3)	0.12753(4)
Co3-1-2	18h	0	0.2492(3)	0
Co3-2-1	18h	-0.16578(16)	0.16578(16)	0.07001(4)
Co3-2-2	6c	0.50090(16)	0.49910(16)	0.09745(4)
Co4-1-1	6c	-0.0006(3)	0.49970(16)	0.13438(4)
Co4-1-2	18h	-0.3333	0.3333	0.12813(7)
Co4-2-1	18h	-0.5	0	0
Co4-2-2	6c	0.3333	0.6667	0.1667
Co5-1-1	18h	-0.24970(16)	0.24970(16)	0.00021(4)
Co5-1-2	6c	0.3333	0.6667	0.06986(7)
Co5-2-1	18h	0.3333	0.6667	0.03187(7)

Co5-2-2	6c	-0.3333	0.3333	0.04011(7)
O1	36i	-0.0734(11)	0.3526(11)	0.15187(14)
O2	18h	-0.0733(8)	0.0733(8)	0.1512(2)
O3	6c	-0.3333	0.3333	0.1529(4)
O4	36i	-0.0021(11)	0.2477(11)	0.04940(14)
O5	36i	-0.0884(11)	0.3231(11)	0.08437(14)
O6	18h	0.1691(8)	0.3382(16)	0.0133(2)
O7	18h	-0.0861(8)	0.0861(8)	0.0154(2)
O8	36i	-0.3271(11)	0.0854(11)	0.01515(14)
O9	18h	0.2405(8)	0.4810(16)	0.1827(2)
O10	18h	0.1647(8)	0.3294(16)	0.1538(2)
O11	18h	-0.2467(8)	0.2467(8)	0.0508(2)
O12	36i	0.3587(11)	0.4285(11)	0.11813(14)
O13	18h	-0.1415(17)	-0.0707(8)	0.1184(2)
O14	18h	0.5736(8)	0.4264(8)	0.1190(2)
O15	18h	-0.0866(8)	0.0866(8)	0.0832(2)
O16	18h	-0.4127(8)	0.1746(16)	-0.0152(2)
O17	6c	-0.3333	0.3333	0.0161(4)
O18	18h	0.2507(8)	0.5015(16)	0.0484(2)
O19	18h	0.4130(8)	0.5870(8)	0.0823(2)

Table 5. Main distances and bond valence calculations for the low temperature structure of $Ba_3Co_{10}O_{17}$

	100K (a_{RT},b_{RT},c_{RT} ;R-3m)						4.9K ($2xa_{RT}$,$2xb_{RT}$,$2xc_{RT}$;R-3m).				
	multi	<Co-O> (Å)	Co2+	Co3+	av		multi	<Co-O> (Å)	BV_{Co2+}	BV_{Co3+}	BV
Co1	3	2.085	2.188	1.885	**2**	**Co1-1-1**	9	2.128	1.93	1.667	**2**
						Co1-1-2	9	2.160	2.51	2.16	**2**
						Co1-2-1	3	2.026	2.48	2.14	**2**
						Co1-2-2	3	2.027	1.71	1.47	**2**

Co2	9	1.917	3.35	2.887	**3**	**Co2-1-1**	18	1.906	3.44	2.96	**3**
						Co2-1-2	18	1.893	3.67	3.16	**3**
						Co2-2-1	18	1.940	3.08	2.66	**3**
						Co2-2-2	18	1.943	3.16	2.73	**3**
Co3	6	2.019	2.57	2.21	**2.5**	**Co3-1-1**	6	2.022	2.46	2.12	**3**
						Co3-1-2	18	2.031	2.39	2.06	**3**
						Co3-2-1	18	2.007	2.84	2.45	**3**
						Co3-2-2	6	2.025	2.98	2.57	**3**
Co4	**6**	**1.930**	**2.67**	**3.01**	**3**	**Co4-1-1**	**6**	**1.845**	**4.14**	**3.57**	**4**
						Co4-1-2	**18**	**1.853**	**3.98**	**3.43**	**4**
						Co4-2-1	18	2.023	2.44	2.11	**3**
						Co4-2-2	6	1.993	2.68	2.31	**3**
Co5	6	1.886	2.45	2.11	**2.5**	**Co5-1-1**	18	1.977	1.92	1.65	**2**
						Co5-1-2	6	1.905	2.29	1.97	**2**
						Co5-2-1	18	1.819	3.02	2.6	**2**
						Co5-2-2	6	1.835	2.86	2.47	**2**

Figure for the TOC: